Sensitivity of LES-based harmonic flame response model for turbulent swirled flames and impact on the stability of azimuthal modes

Michaël Bauerheim, Gabriel Staffelbach, Nick A. Worth, James Dawson, Laurent Y.M. Gicquel, Thierry Poinsot

Sensitivity of LES-based harmonic flame response model for turbulent swirled flames and impact on the stability of azimuthal modes

M. Bauerheim [a,b,*], G. Staffelbach [a], N.A. Worth [c], J.R. Dawson [c], L.Y.M. Gicquel [a], T. Poinsot [d]

[a] *CERFACS, CFD team, 42 Av Coriolis, 31057 Toulouse, France*
[b] *Société Nationale d'Etude et de Construction de Moteurs d'Aviation, 77550 Reau, France*
[c] *NTNU, Department of Energy and Process Engineering, 7491 Trondheim, Norway*
[d] *Institut de Mécanique des Fluides de Toulouse, INP de Toulouse and CNRS, Avenue C. Soula, 31400 Toulouse, France*

Abstract

This paper describes a numerical study of azimuthal unstable modes in the annular combustor of Cambridge. LES is used to compute a Harmonic Flame Response Model (HFRM) and a Helmholtz solver to predict the overall stability of the combustor. HFRM quantifies the interaction between acoustics and the turbulent swirled flames. They must be known with precision because instabilities are very sensitive to subtle changes. The effects of azimuthal confinement (corresponding to the annular combustor equipped with 12 or 18 burners), thermal boundary conditions and fuel type (methane or ethylene) on HFRMs are simulated here using LES of a single 20 degree ($N = 18$) or 30 degree ($N = 12$) sector. A double-sector LES is also computed to investigate flame/flame interactions. These LES-based HFRMs are then used as inputs for a Helmholtz solver and results show that (1) subgrid-scale LES models lead to marginal effects on the harmonic flame response while (2) azimuthal confinement, thermal conditions and fuel type strongly affect the flame response to acoustics and therefore control the stability of the azimuthal mode. Computations show that the annular experiment performed with methane should be stable while ethylene should lead to azimuthal unstable modes as observed experimentally.

Keywords: Sensitivity; HFRM; Instabilities; Azimuthal mode; LES

1. Introduction

Thermo acoustic instabilities often prevent easy and fast commissioning of new designs of power generation as well as aeronautical gas turbine engines [1,2]. Operating conditions leading to instabilities are currently impossible to predict *a priori* and are usually only discovered during full

* Corresponding author. Address: CERFACS, CFD Team, 42 Avenue G. Coriolis, 31057 Toulouse Cedex 01, France. Fax: +33 (0)5 61 19 30 00.
E-mail address: bauerheim@cerfacs.fr (M. Bauerheim).

http://dx.doi.org/10.1016/j.proci.2014.07.021

engine testing. Thermo-acoustic instabilities result from the coupling of unsteady combustion and acoustic eigenmodes of the geometry. In the annular chambers of gas turbines, azimuthal modes are the most common and difficult to control [3]. Three tools are available today to simulate azimuthal modes and complement full annular laboratory scale rigs [4–7]: unsteady CFD [8], thermo-acoustic solvers [9] and reduced order models [10,11]. Although the three approaches are clearly essential for our understanding, the combination of full annular rig test facilities and Large Eddy Simulations is the best method to address the underlying mechanisms [12].

Because of their extreme costs, computations of full 360° configurations are still out of reach today and not designed to study underlying phenomena leading to combustion instabilities. To develop predictive tools and determine the stability of a given design point, a reduced strategy is used: (1) A Harmonic Flame Response Model (HFRM), Flame Transfer Function (FTF, [13]) or Flame Describing Functions (FDF, [14]) can be evaluated numerically to link the flame response to acoustics. To do so, only one sector with periodic and non-reflecting boundary conditions is computed using LES since the capture of a self-excited azimuthal mode is not required [15,16]. (2) The acoustic/flame model (HFRM) is then introduced as a source term in a full annular acoustic solver, much cheaper than LES, to study the azimuthal acoustic mode in the complete 360° configuration. Although successful in determining the stability of real burners [9] such coupled approaches are known to be sensitive to multiple parameters [17].

This paper intends to evaluate the robustness of this LES-Helmholtz strategy to determine HFRM using LES and inject them as inputs of a Helmholtz solver to predict the stability of the annular test rig of Cambridge [4,5]. Section 2 describes the annular rig of Cambridge. In Section 3, the numerical strategy and the various cases used to evaluate the HFRM (Section 3.1) and stability (Section 3.2) are defined. Results on mean and phase-averaged flow fields for unforced and forced cases are discussed and compared to experiment in Sections 4.1 and 4.2. Section 4.4 focuses on the HFRM sensitivity to various LES sub models as well as key phenomena (azimuthal confinement, thermal conditions and fuel type) affecting the flow dynamics and flame shape as observed in previous sections. Finally, Section 4.5 gives the stability map of the 360° configuration. The impact of azimuthal confinement, thermal conditions and fuels on the stability is assessed: the annular rig is found to be stable when using methane while ethylene leads to azimuthal instabilities as observed in the annular experiment [4,5].

2. Target configuration: the full annular combustor of [4]

The target experiment is the annular combustor of Cambridge studied by [4] (Fig. 1: for detailed descriptions of the apparatus and experimental methods see [4,5]). The stainless steel rig can include $N = 12, 15,$ or 18 equally spaced flames around a circumferential diameter of 170 mm. Premixed reactants are supplied by a common plenum which includes grids and flow straighteners for flow conditioning and acoustic damping. For all configurations, mass flow controllers are used to maintain a constant bulk velocity of $U = 18\ \mathrm{m\ s^{-1}}$ at the exit of each bluff body. This ensures that any changes in the flame structure and dynamics are a result of azimuthal confinement (flame spacing). The rig is instrumented with microphones to characterize the instability modes and a high-speed intensified camera is used to measure the OH^* chemiluminescence of the whole annulus.

To find a set of conditions that give rise to self-excited azimuthal modes, the inner (L_i) and outer (L_o) lengths of the combustor walls, azimuthal confinement, and two fuel types (CH_4 and C_2H_4) were varied in the experiment [4,5]: strong self-excited azimuthal modes only occurred for C_2H_4–air mixtures and when different inner and outer tube lengths $L_i = 130$ mm and $L_o = 300$ mm were used. [6] also found that L_i and L_o must be different to excite azimuthal modes. The occurrence of self-excited azimuthal modes did not depend on azimuthal confinement but the limit-cycle amplitude and the flame structure did. Only longitudinal modes were observed for CH_4-air mixtures.

3. Numerical models

3.1. Large eddy simulations

Large Eddy Simulation (LES) of compressible flow is widely recognized as an accurate method [1] to study combustion instabilities in complex configurations [8,18–20] but the impact of subgrid scale models on LES results for instabilities is rarely discussed. To study the impact of these models on HFRM computations, a fully compressible explicit code (called AVBP) is used to solve the filtered multi-species 3D Navier–Stokes equations with realistic thermochemistry on unstructured meshes [21,22]. Numerics is based on a two-step Taylor–Galerkin finite element scheme of third-order in space and time (TTGC, [23]) to accurately propagate acoustic waves. Boundary conditions use the NSCBC approach [24] and ensure non-reflecting conditions [25] as well as the proper introduction of acoustic waves in the LES domain for HFRM computations.

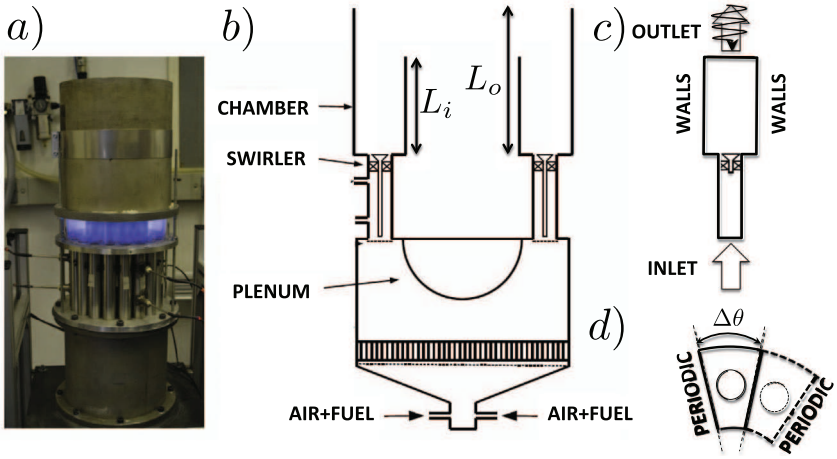

Fig. 1. Photograph (a) and schematic (b) of the annular experiment with $L_i = 130$ mm and $L_o = 300$ mm complemented by a longitudinal (c) and a transverse (d) cut of the single (——) and double (- - -) sector computation domain.

The sensitivity of HFRM predictions to different sub-grid stress models is tested using the classical Dynamics Smagorinsky model [26] and both the Wale [27] and Sigma [28] models. Turbulent-flame interactions are addressed using the dynamic Thickened Flame (TF) approach with two different efficiency functions as a performance test: the Colin model [29] and the Charlotte-Meneveau model [30]. These combustion models are closed by approximating the subgrid scale turbulent velocity u'_Δ with an operator based on the rotational of the velocity field to remove the dilatation part of the velocity.

Although HFRM estimations can be obtained from an acoustically isolated single sector of a real configuration, flow confinement is known to play a role on flame shape and stability. The effect of confinement and flame/flame interactions was tested here by comparing single and double sector LES (Fig. 1, d). All computational domains include the axial swirler composed of six blades mounted on a bluff-body (Figs. 2 and 3).

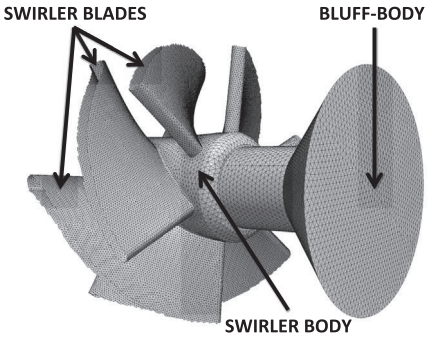

Fig. 2. 3D view of the swirler and the associated surface mesh.

Since the overall number of injectors N also varies, different angles, $\Delta\theta = 30°$ or $20°$, are considered for the single-sector cases, corresponding respectively to the annular rig equipped with $N = 12$ or $N = 18$ burners (Fig. 1). All meshes are fully unstructured and contain 4.2 millions cells (for the case $\Delta\theta = 20°$) or 5.5 million cells (for $\Delta\theta = 30°$) per sector for the coarse cases while the refined case contains 31 million cells. This results in typical thickening factors of 3 to 5 in the flame zone to guarantee $5 - 10$ points in the flame. Cells lengths are typically 80 μm near swirler walls and 150 μm in the swirler passages.

An axial acoustic forcing is performed in the LES to compute HFRMs since the main mechanism leading to azimuthal combustion instabilities is the modulation of the axial mass flow rate through the injectors. Transverse acoustic forcing [31,32] is not considered here since it only characterizes flames located at a pressure node which do not contribute to the stability of the system.[1] The forcing frequency corresponds to the azimuthal mode observed experimentally [4] ($f \simeq 1800$ Hz) and is introduced in the LES by pulsating (with the NSCBC approach) the outlet ingoing acoustic wave of the sector (Figs. 1 and 3). No data on the forcing amplitude is reported since the experiment is self-excited: in the LES, various low amplitudes (ensuring $p'/\bar{p} < 1$) of the forcing wave have been tested and no impact on the HFRM was observed.

HFRMs are constructed by recording the global heat release rate $\dot{Q}'_i(t)$ and the reference acous-

[1] The Rayleigh criterion is proportional to $\|\hat{p}\|\|\hat{q}\|$ thus flames at pressure nodes ($\|\hat{p}\| = 0$) lead to a null Rayleigh term and therefore do not contribute to the stability of the system.

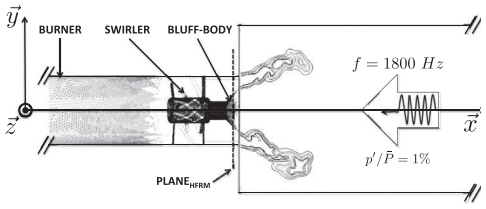

Fig. 3. XY-cut of the single-sector configuration with iso-contours of heat release. Acoustic enters the domain via the forced outlet.

tic velocity $u'_{REF}(t)$ [13]. This velocity is obtained by averaging the axial fluctuating velocity over a plane (Plane$_{HFRM}$in Fig. 3).

Based on the experiments [4], a perfectly premixed air–fuel mixture (methane or ethylene) at the equivalence ratio $\phi = 0.85$ is injected in the inlet (plenum/burner section). [4] mention that using ethylene (C_2H_4) leads to azimuthal instabilities while only longitudinal modes appear with methane (CH_4). These two fuels are investigated here with LES. Reaction rates are modeled with reduced kinetic schemes, which have been proved to accurately reproduce low frequency flame dynamics [36]: 1 reaction, 4 species for CH_4 and 2 reactions, 6 species for C_2H_4. Adiabatic temperatures and laminar flame speeds have been compared to GRIMECH [33] for methane and UCSD full schemes [34] for ethylene.

Thermal effects also modify HFRMs [17,35]: here, adiabatic as well as heat-loss formulations were applied on the chamber walls. For the heat loss formulation, the heat flux imposed on a wall is locally expressed as $\Phi = (T - T_\infty)/R_w$ where the temperature T_∞ is set to 600 K and the thermal resistance is $R_w = 10^{-4}(\mathrm{Km}^2)/\mathrm{W}$. For these values, the chamber walls typically reach 1000 K.

For all computed cases (Table 1), as in the experiment, the mean axial velocity at the burner/chamber junction is conserved: 18 m s^{-1}.

3.2. Helmholtz simulations of the full annular combustor

A full 3D acoustic solver called AVSP [9] is used to predict the effect of the HFRM on the stability of the azimuthal mode observed experimentally at $f \simeq 1800$ Hz. AVSP solves the eigenvalues problem issued from a discretization on unstructured meshes (with 3.6 millions cells) of the wave equation where the source term due to combustion is expressed using HFRMs [13]. The local reaction term $\dot{Q}'_i$ is expressed for each burner i as:

$$\widehat{\dot{Q}'}_i = n_{u,i}\, e^{j\omega\tau_i}\, \widehat{u'}(\mathbf{x}_{ref,i}) \tag{1}$$

where $\widehat{u'}(\mathbf{x}_{ref,i})$ is the Fourier transform of the axial acoustic velocity component at the location $\mathbf{x}_{ref,i}$. The interaction index $n_{u,i}$ is constant for each sector i in the flame zone (Fig. 4) and its value is chosen to recover the global value of unsteady heat release [9] computed by LES. It is set to zero outside of the flame zone.

The acoustic domain computed with AVSP is the 360° configuration with $N = 12$ or 18 burners connected to the plenum (Fig. 4). Different lengths are used for the inner and outer chamber walls ($L_i = 130$ mm and $L_o = 300$ mm) [5,6]. Infinite impedances (corresponding to $u' = 0$) are applied on walls or plenum inlet and a pressure node ($p' = 0$) is applied at the outlet. Mean density and sound speed are extracted from LES simulations of the single-sector and replicated azimuthally for all sectors.

4. Results and discussions

4.1. Mean unforced flow fields

A first indication of the effects of parameter changes on LES results is provided by unforced reactive LES predictions on a single-sector (or double sector in the DOUBLE case, Table 1) of the annular rig. Streamlines from the averaged

Table 1
Several cases to investigate the HFRM sensitivity.

Case	Comb.	Turb.	Sector	Mesh	Therm.	$\Delta\theta$	Fuel
Ref	Charlette	Wale	1	Coarse	Adiabatic	20	CH_4
Colin	**Colin**	Wale	1	Coarse	Adiabatic	20	CH_4
Smago	Charlette	***Smago***	1	Coarse	Adiabatic	20	CH_4
Sigma	Charlette	***Sigma***	1	Coarse	Adiabatic	20	CH_4
Double	Charlette	Wale	**2**	Coarse	Adiabatic	20	CH_4
Fine	Charlette	Wale	1	***Fine***	Adiabatic	20	CH_4
CH4-HL-20	Charlette	Wale	1	Coarse	**Heat-loss**	20	CH_4
C2H4-ADIA-20	Charlette	Wale	1	Coarse	Adiabatic	20	$\boldsymbol{C_2H_4}$
CH4-ADIA-30	Charlette	Wale	1	Coarse	Adiabatic	**30**	CH_4
CH4-HL-30	Charlette	Wale	1	Coarse	***Heat-loss***	**30**	CH_4
C2H4-ADIA-30	Charlette	Wale	1	Coarse	Adiabatic	**30**	$\boldsymbol{C_2\ H_4}$

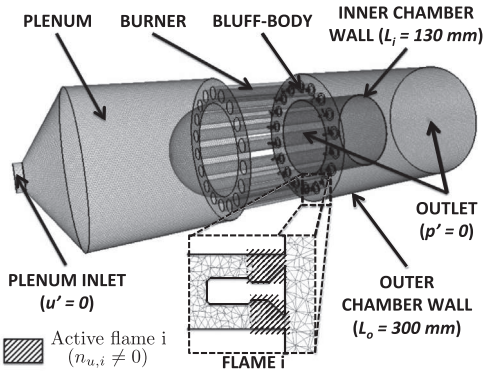

Fig. 4. 3D view to the 360° acoustic domain with $N = 18$ burners and zoom on the *ith* flame zone.

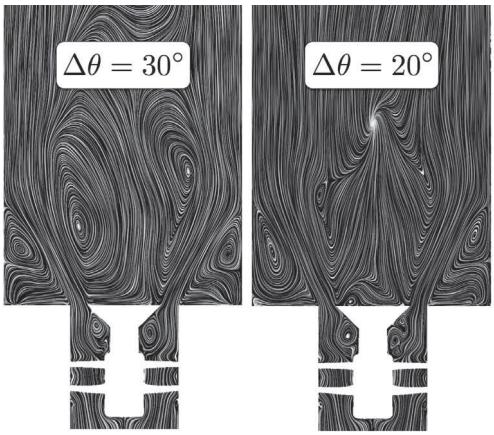

Fig. 5. Averaged streamlines visualized by Line Integral Convolution (LIC) [37] on the XY-plane for the CH4-ADIA-30 ($\Delta\theta = 30°$, left) and REF ($\Delta\theta = 20°$, right) non-pulsed cases.

flow fields are visualized by Line Integral Convolution (LIC) [37] in Fig. 5 for the $\Delta\theta = 20°$ (right) and 30° (left) cases. They confirm that the distance between neighboring sectors deeply affects the aerodynamics, especially the central recirculation zone, and therefore the flame shape.

On the contrary, taking heat losses into account or changing fuel has only a minor impact on aerodynamics. However, the flame anchoring point is slightly lifted (Fig. 6, middle) when heat losses are taken into account and the local heat release increases when methane is replaced by ethylene (Fig. 6, right).

The flame shapes obtained by LES (heat-release fields and iso-contours 20 mm downstream of the bluff-body, Fig. 7 top) with $\Delta\theta = 20°$ and $\Delta\theta = 30°$ are compared to the experimental integrated chemiluminescence results provided by [4] (Fig. 7, bottom). LES and experiment are in good

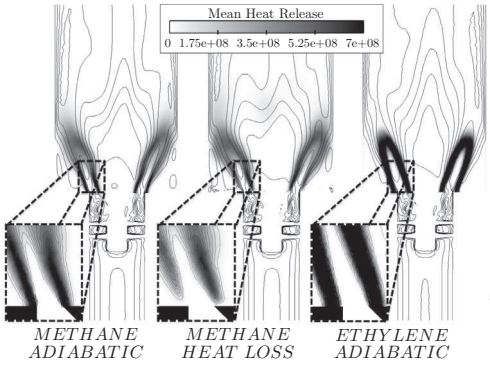

Fig. 6. XY-cuts of the mean heat release with iso-contours of mean axial velocity for the REF case (left), CH4-HL-20 case (middle) and C2H4-ADIA-20 case (right). Zoom on heat release fields for each flame is provided to highlight the flame anchoring point.

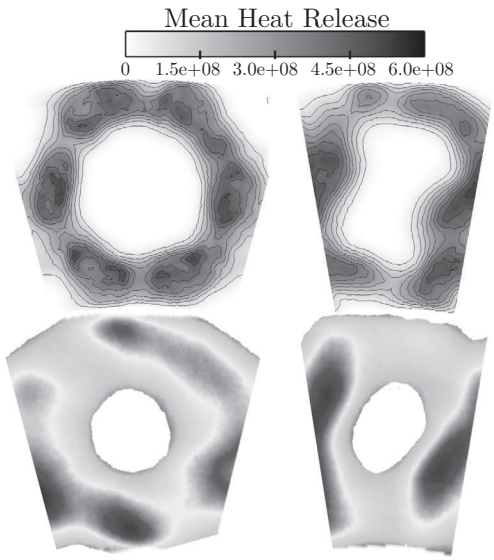

Fig. 7. Heat release fields and iso-contours 20 mm downstream of the bluff-body (LES, top) and integrated OH^* (experiment [4], bottom) for the C2H4-ADIA-30 case (left) and the C2H4-ADIA-20 case (right).

agreement: the inner flame wrinkling and the outer flame merging are observed in both LES and experiment in the $\Delta\theta = 20°$ case. Burner/burner interactions clearly appear for $\Delta\theta = 20°$ where the flames are not axisymmetric.

4.2. Phase averaged forced flow fields

The response of the forced flames can be visualized by the averaged heat release rate at different phase angles of the pressure oscillation: 0° and 180° correspond to a zero acoustic pressure varia-

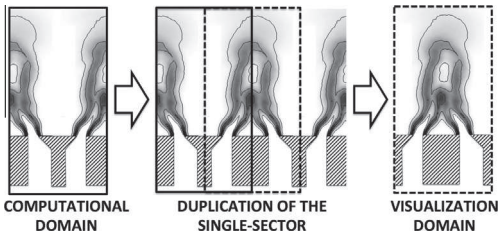

Fig. 8. Computation domain (left) and visualization domain (right) used to study flame-flame interactions.

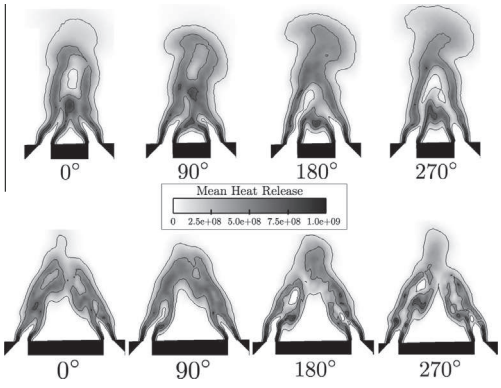

Fig. 9. XZ-cuts of phase averaged heat release in two consecutive mid injector planes: REF case ($\Delta\theta = 20°$, top) and CH4-ADIA-30 case ($\Delta\theta = 30°$, bottom).

tion at the outflow while 90° and 270° correspond to the maximum and minimum pressure levels respectively. To focus on the flame/flame interaction, the visualization domain differs from the single-sector computational domain (Fig. 8). As evidenced by Fig. 9, flame merging is the main consequence of external forcing for both cases.

Figure 10 shows that the introduction of a model for heat losses strongly modifies the flame shape. Contrarily to adiabatic cases, the flame is lifted, has a weaker branch outer shear layer flame [35] and its base oscillates near the injector tip as already evidenced for laminar premixed flames [36]. The outer branch oscillates in the axial direction while the inner branch located nearby the bluff-body moves from left to right (—— in Fig. 10 displays the minimum and maximum flame position over the acoustic period).

Replacing methane by ethylene (Table 1) impacts the flame dynamics (Fig. 11). For ethylene (runs C2H4-ADIA-20 and C2H4-ADIA-30), the laminar flame speed ($s^0_{l,C_2H_4} \simeq 0.56$ m/s) and the heat release (as well as the adiabatic temperature $T^{ad}_{C_2H_4} \simeq 2232$ K) are higher compared to methane ($s^0_{l,CH_4} \simeq 0.33$ m/s and $T^{ad}_{CH_4} \simeq 2070$ K) leading to a shorter and more intense flame (Fig. 9 for methane and Fig. 11 for ethylene). Because of a smaller flame length, ethylene flame

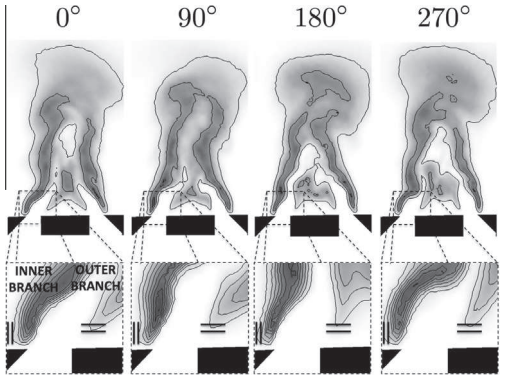

Fig. 10. XZ-cuts of the phase averaged heat release (same color levels as in Fig. 9) for the CH4-HL-20 case (top) complemented by a zoom on the flame base oscillation (bottom). ——: Minimum/maximum position of the inner and outer flame base.

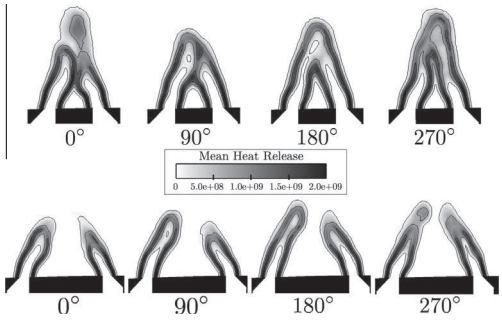

Fig. 11. XZ-cuts of the phase averaging of the heat release in the C2H4-ADIA-20 case (top) and C2H4-ADIA-30 case (bottom).

merging between neighboring injectors occurs only in the $\Delta\theta = 20°$ case and disappears for $\Delta\theta = 30°$ which is consistent with experimental observations [4] (while merging was only weaker for methane with $\Delta\theta = 30°$ compared to $\Delta\theta = 20°$).

4.3. Rayleigh criterion

First, to analyze the stability of the configuration and compare methane and ethylene cases, the Rayleigh criterion (R_S) over any surface S is computed from the complex fluctuating pressure ($\hat{p}$) and heat release ($\hat{q}$):

$$R_S = \frac{1}{S}\int_S \|\hat{p}\|\|\hat{q}\|\cos(\Phi_p - \Phi_q)dS \qquad (2)$$

where $\|\hat{p}\|$ and $\|\hat{q}\|$ are the modulus of the pressure and heat release oscillations and Φ_p and Φ_q are their respective phases. The fluctuating quantities are obtained at the forcing frequency thanks to a Dynamic Mode Decomposition (DMD) [37] of

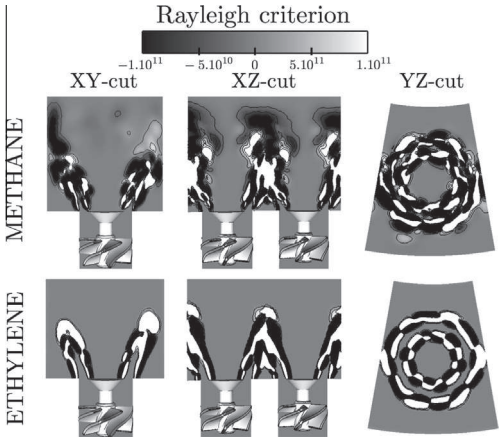

Fig. 12. Rayleigh criterion (Eq. (2)) over three different surfaces for the adiabatic $\Delta\theta = 20°$ case with methane (top) and ethylene (bottom).

Table 2
Rayleigh criterion (Eq. (2)) for the adiabatic $\Delta\theta = 20°$ cases with methane and ethylene over two different surfaces: XY-cut where flame-wall interaction occurs and XZ-cut where flame merging is observed. It suggests that flame merging would stabilize the configuration with both methane and ethylene.

CASE	XY-CUT	XZ-CUT
Methane	−3270 W	−621 W
Ethylene	+5315 W	−1268 W

110 3D snapshots spaced by $\Delta t = 27$ µs (corresponding to five periods and a Nyquist cutoff frequency $f_n = 37$ kHz). Figure 12 shows the Rayleigh criterion for the adiabatic methane (top) and ethylene (bottom) cases with $\Delta\theta = 20°$ over three different surfaces. Especially, the YZ-cut (right) highlights the swirler (with 6 blades) effect on stability with the 6*th*-order azimuthal pattern observed while the XY and XZ-cuts display the flame-wall (left) and flame-flame (middle) interactions effect: values of the Rayleigh criterion are provided in Table 2 to compare these two interactions. Table 2 shows that flame merging stabilizes (negative Rayleigh criterion) the configuration with both methane and ethylene. However, a positive criterion is obtained with ethylene on the other direction (XY-cut). Using methane (lower flame speed) leads to a longer flame which promotes flame-wall interaction. As observed in Fig. 12, a negative criterion is obtained near walls which indicates that flame-wall interaction with methane would stabilize the configuration.

4.4. HFRM sensitivity study

Sensitivity of HFRMs to models (turbulence and combustion) as well as numerical setups (single/double sectors and coarse/fine meshes) is first evaluated for adiabatic cases with methane and $\Delta\theta = 20°$ (REF, DOUBLE, COLIN, SIGMA and FINE cases, Fig. 13). Hatched zones in Fig. 13 correspond to the minimum and maximum values of n and τ for these 5 cases. Results depend only weakly on modeling parameters for amplitudes n and time-delays τ of the HFRM (five first cases in Fig. 13): the amplitude n changes from 0.175 to 0.29 while τ varies between 0.29 ms and 0.34 ms.

Thermal, azimuthal confinement ($\Delta\theta = 20°$ or 30°) and fuel effects were found to have strong impact on unforced (Section 4.1) and forced (Section 4.2) flames. For HFRMs, the CH4-HL-20, CH4-ADIA-30, CH4-HL-30 and C2H4-ADIA-20 results (Fig. 13) confirm that confinement, thermal and fuel effects are significant compared to uncertainties coming from LES sub-models (hatched zones in Fig. 13):

- **Azimuthal confinement:** Using $\Delta\theta = 30°$ instead of 20° modifies the flow topology (Fig. 5) and the flame merging (Fig. 9) which leads to a significant amplification of the acoustic/combus-

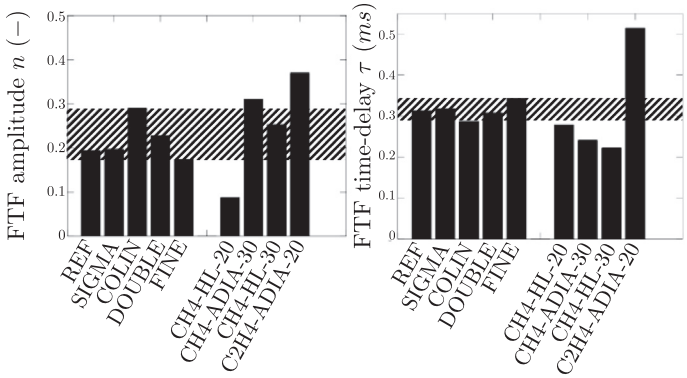

Fig. 13. HFRM amplitudes n and time-delays τ computed by LES for cases of Table 1.

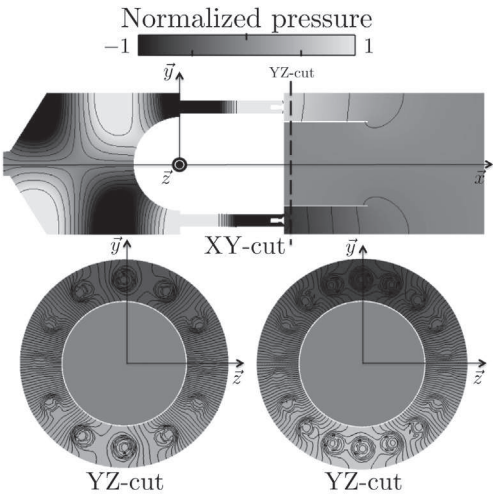

Fig. 14. Mode structure (here $\|p'\|\cos(\phi)$) of the azimuthal mode at $f \simeq 1800$ Hz: XY-cut (top) and YZ-cuts (bottom) for both the $N = 12$ (left) and $N = 18$ (right) configurations.

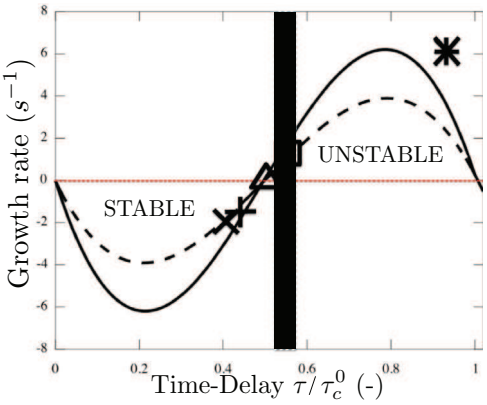

Fig. 15. Stability maps of the $N = 12$ (---) and $N = 18$ (——) configurations obtained with the HFRM amplitude $n = 0.25$ and a time-delay varying from 0 ms to $\tau_c^0 = 0.55$ ms. Growth rates of specific cases are also displayed: □: REF case, △: CH4-HL-20, +: CH4-ADIA-30, ×: CH4-HL-30 and ☆: C2H4-ADIA-20. The hatched zone corresponds to the uncertainty on the time-delay due to LES sub models (Fig. 13).

tion interactions (the amplitude of the HFRM n increases) and a shorter flame response (the time-delay τ decreases).

- **Thermal effect:** Including heat-losses modifies the flame shape and introduces flame base oscillations (Fig. 10) which are not present for adiabatic LES: both the HFRM amplitude n and time-delay τ decrease. This behavior is consistent with other studies on longitudinal configurations [35].
- **Fuel effect:** Methane and ethylene lead to completely different flame responses. The delay with C_2H_4 increases to 0.51 ms compared to about 0.3 ms for CH_4, everything else being equal.

4.5. Effect of HFRM uncertainties on the stability of azimuthal modes

Variabilities in HFRM numerical estimations have been clearly identified but their impact on the burner stability predictions is not yet evidenced. Helmholtz simulations are now performed using computed HFRM to investigate the global stability of the 360° configuration (Fig. 4). Stability maps relying on the growth rate $Im(f)$ function of the time-delay τ (varying from 0 to $\tau_c^0 = 1/1800 \simeq 0.55$ ms) are first computed for two baseline cases corresponding to the annular rig equipped with $N = 12$ burners ($\Delta\theta = 30°$) or 18 burners ($\Delta\theta = 20°$) and using $n = 0.25$ (estimation of an adiabatic case with methane, Fig. 13).

The mode structure (*i.e.* $\|p'\|\cos(\phi)$ where $\phi = arg(p')$) of the azimuthal mode at $f \simeq 1800$ Hz obtained with AVSP (Fig. 14,, top) involves both the annular plenum as well as the annular chamber. A longitudinal acoustic component is observed in the chamber because of pressure fluctuations are zero at the chamber outlet. YZ-cuts of the $N = 12$ and 18 burner cases (Fig. 4,, bottom) underline the differences introduced in the acoustic mode due to the number of burners as well as to the HFRM [38].

Figure 15 shows the stability maps of the two baseline cases (--- : $N = 12$ and —— : $N = 18$ burner configurations) versus HFRM time-delay τ, computed first with $n = 0.25$ (corresponding to an adiabatic case with methane). Results confirm that the azimuthal confinement modifies the acoustic domain leading to different growth rates, everything else being equal: using the same burner characteristics and HFRM inputs, the 12 burner case generates lower flame/acoustic perturbations than the 18 burner case (Fig. 14 bottom).

Finally, the growth rate of the five distinct cases of interest are displayed on the stability map of Fig. 15 (□: REF case, △: CH4-HL-18, +: CH4-ADIA-12, ×: CH4-HL-12 and ☆: C2H4-ADIA-18): thermal and fuel effects have a significant impact on the overall stability compared to uncertainties due to LES sub-models (hatched zone in Fig. 15). Results demonstrate the LES capability to predict HFRM accurately. When these HFRMs are used in the Helmholtz solver, almost all methane cases are stable and adding heat-losses stabilizes (in these cases) the annular rig. However, using ethylene leads to a positive growth corresponding to an unstable configuration. These results are consistent with experimental observations where methane leads only to

longitudinal instabilities while ethylene produces azimuthal instabilities [4].

5. Conclusion

This paper describes a sensitivity analysis of the stability of a full annular academic configuration installed in Cambridge. It is based on forced compressible LES of a single (or double) sector computed HFRM which quantify the interaction between acoustics and the turbulent swirled flames. First, effects of different azimuthal confinements (corresponding to the annular chamber equipped with 12 or 18 burners), thermal boundary conditions (adiabatic or with heat losses) or fuels (methane or ethylene) have been investigated and compared to uncertainties on the HFRM introduced by LES sub models. Phase-averaged heat release fields and HFRM computations show that confinement, thermal and fuel effects are essential and affect the flame shape as well as their dynamics. HFRM computed by LES are used as inputs for an acoustic solver to evaluate the effect of HFRM uncertainties on the stability of azimuthal modes in the 360° configuration. Results show that modeling issues inherent to LES models lead to marginal uncertainties on HFRM while azimuthal confinement, thermal conditions and fuel type strongly affect the flame response to acoustics and control the stability of the azimuthal mode. In particular, computations show that the annular configuration performed with methane should be stable while ethylene should lead to unstable modes as observed in the real experiment.

References

[1] T. Poinsot, D. Veynante, Theoretical and Numerical Combustion, third ed. (<www.cerfacs.fr/elearning>), 2011.
[2] T. Lieuwen, A. Banaszuk, *J. Propul. Power* 21 (1) (2005) 25–31.
[3] W. Krebs, P. Flohr, B. Prade, S. Hoffmann, *Combust. Sci. Tech.* 174 (2002) 99–128.
[4] N. Worth, J. Dawson , *Proc. Combust. Inst.* (2013) 3127–3134.
[5] N. Worth, J. Dawson, *Combust. Flame* 160 (11) (2013) 2476–2489.
[6] J.-F. Bourgouin, D. Durox, J. Moeck, T. Schuller, S. Candel, in: ASME Turbo Expo, GT2013-95010, 2013.
[7] J. Moeck, M. Paul, C. Paschereit, in: ASME Turbo Expo 2010 GT2010-23577, 2010.
[8] P. Wolf, G. Staffelbach, L. Gicquel, J. Muller, T. Poinsot, *Combust. Flame* 159 (2012) 3398–3413.
[9] F. Nicoud, L. Benoit, C. Sensiau, T. Poinsot, *AAAI* 45 (2007) 426–441.
[10] C. Pankiewitz, A. Fischer, C. Hirsch, T. Sattelmayer, in: AIAA-2003-3295 (Ed.), 9th AIAA/CEAS Aeroacoustics Conference & Exhibit, Hilton Head, SC, USA, 2003.
[11] A.P. Dowling, *J. Sound Vib.* 180 (4) (1995) 557–581.
[12] L. Gicquel, G. Staffelbach, T. Poinsot, *Prog. Energy Combust. Sci.* 38 (6) (2012) 782–817.
[13] L. Crocco, *J. Am. Rocket Soc.* 21 (1951) 163–178.
[14] N. Noiray, D. Durox, T. Schuller, S. Candel, *J. Fluid Mech.* 615 (2008) 139–167.
[15] A. Giauque, L. Selle, T. Poinsot, H. Buechner, P. Kaufmann, W. Krebs, *J. Turbul.* 6 (21) (2005) 1–20.
[16] R. Kaess, W. Polifke, T. Poinsot et al., in: Proceedings of the Summer Program, Center for Turbulence Research, NASA AMES, Stanford University, USA, pp. 289–302, 2008.
[17] F. Duchaine, L. Selle, T. Poinsot, *Combust. Flame* 158 (12) (2011) 2384–2394.
[18] A. Sengissen, A. Giauque, G. Staffelbach, et al., *Proc. Combust. Inst.* 31 (2007) 1729–1736.
[19] C. Fureby, *Flow, Turbul. Combust.* 84 (2010) 543–564.
[20] G. Kuenne, A. Ketelheun, J. Janicka, *Combust. Flame* 158 (9) (2011) 1750–1767.
[21] T. Schønfeld, T. Poinsot, in: Proceedings of the Summer Program, Center for Turbulence Research, NASA Ames/Stanford Univ., 1999, pp. 73–84.
[22] S. Roux, G. Lartigue, T. Poinsot, U. Meier, C. Bérat, *Combust. Flame* 141 (2005) 40–54.
[23] V. Moureau, G. Lartigue, Y. Sommerer, C. Angelberger, O. Colin, T. Poinsot, *J. Comput. Phys.* 202 (2) (2005) 710–736.
[24] T. Poinsot, T. Echekki, M.G. Mungal, *Combust. Sci. Tech.* 81 (1-3) (1992) 45–73.
[25] L. Selle, F. Nicoud, T. Poinsot, *AAAI* 42 (5) (2004) 958–964.
[26] J. Smagorinsky, *Monthly Weather Rev.* 91 (1963) 99–164.
[27] F. Nicoud, F. Ducros, *Flow, Turbul. Combust.* 62 (3) (1999) 183–200.
[28] F. Nicoud, H. Baya-Toda, O. Cabrit, S. Bose, J. Lee, *Phys. Fluids* 23 (085106) (2011) 1–12.
[29] O. Colin, F. Ducros, D. Veynante, T. Poinsot, *Phys. Fluids* 12 (7) (2000) 1843–1863.
[30] F. Charlette, D. Veynante, C. Meneveau, *Combust. Flame* 131 (2002) 159–180.
[31] J. O'Connor, T. Lieuwen, *Phys. Fluids* 24 (2012), 075107.
[32] F. Lespinasse, F. Baillot, T. Boushaki, *Comptes rendus de l'Académie des Sciences – Mécanique* 341 (2013) 110–120.
[33] M. Frenklach, H. Wang, M. Goldenberg et al., GRI-Mech: an optimized detailed chemical reaction mechanism for methane combustion, Technical Report GRI-Report GRI-95/0058, Gas Research Institute, 1995.
[34] chemical-kinetic mechanisms for combustion applications, san diego mechanism web page, ucsd. 2013. URL: <http://combustion.ucsd.edu>.
[35] L. Tay-Wo-Chong, W. Polifke, in: ASME Paper 2012-GT-68796, 2012.
[36] K. Kedia, H. Altay, A. Ghoniem, *Proc. Combust. Inst.* 33 (2011) 1113–1120.
[37] B. Cabral, L. Leedom, *in: Proceedings of the 20th Annular Conference on Computer Graphics and Interactive Techniques*, Anaheim, California, 1993, pp. 263–270,.
[37] P. Schmid, *J. Fluid Mech.* 656 (2010) 5–28.
[38] M. Bauerheim, J. Parmentier, P. Salas, F. Nicoud, T. Poinsot, *Combust. Flame* 161 (5) (2014) 1374–1389.